Single ionization of H_2O and C_4H_8O by electron impact: Single-center description of the final state

Emiliano Acebal [*] and Sebastian Otranto [†]

Instituto de Física del Sur (IFISUR), Departamento de Física, Universidad Nacional del Sur (UNS), CONICET, Av. L. N. Alem 1253, B8000CPB - Bahía Blanca, Argentina

(Received 5 April 2024; accepted 29 May 2024; published 13 June 2024)

In this work, we report triple differential cross sections for the single ionization of H_2O and C_4H_8O by electron impact at intermediate to low impact energies, calculated within the framework of the CDW-EIS model considering two different approximations to the continuum electrons' interaction with the molecular ion in the final state. These calculations are benchmarked with recently reported experimental data and two state-of-the-art theoretical models. Present results suggest that a spherical average of the anisotropic potential associated to the residual ion improves the description of these collision processes for electron emission into the scattering and perpendicular planes, with respect to approximating it as a single center of charge +1, whereas full-perpendicular emission is best described by this simpler approximation.

DOI: 10.1103/PhysRevA.109.062807

I. INTRODUCTION

The description of the single ionization of molecules by electron impact represents a challenging scenario in atomic and molecular physics, given that these processes play an important role in biological and astrophysical contexts. More recently, understanding their dynamics has gained relevance in applications for radiobiology, diagnoses by medical images, and radiotherapy. This owes to the fact that the high-energy ionizing radiation generates a great number of secondary electrons that can damage the DNA molecules, due to the temporarily attachment of these electrons to the DNA components [1–3], or when these electrons ionize adjacent H_2O molecules [4].

The dynamics of those processes can be completely analyzed by means of triple differential cross sections (TDCS), which are a function of every kinematic parameter of the collision, except the spin. From an experimental perspective, TDCS for the single ionization of molecules by electron impact have been reported since the 1970s (see Refs. [5–11] among others). However, the H_2O molecule was first studied only two decades ago by Milne-Brownlie and coworkers at an impact energy of 250 eV and for an asymmetric emission [12]. In subsequent years, the symmetric emission regime into perpendicular directions and at lower impact energies was analyzed [13,14]. More recently, two three-dimensional kinematic complete experiments were performed reporting internormalized TDCS at 81 eV [15] and absolute TDCS at 65 eV [16]. These recent experimental reports were achieved with the use of a reaction microscope, specially designed for electron scattering in 2003 [17] and recently updated with a pulsed electron beam source [18,19].

Regarding the C_4H_8O molecule (tetrahydrofuran or THF), it is worth mentioning that this particular target does not directly intervene in biological processes, but can be regarded as a molecular analog to the deoxyribose sugar, which is part of the backbone of the DNA strands. In this sense, experimental TDCS for the single ionization of THF by electron impact were first reported 14 years ago [20,21] as a first step to study collision processes involving DNA backbone components. In 2014, Ren and coworkers studied the fragmentation of THF at an impact energy of 26 eV, observing that the $C_4H_8O^+$ cation without dissociation arise only from the ionization of the highest occupied molecular orbital (HOMO) [18]. In subsequent years, the same group reported TDCS at 91 eV [22], 65 eV [16], and 250 eV [23] for the single ionization of this molecule.

From a theoretical point of view, the models used to analyze electron collisions with H_2O and C_4H_8O targets at the fully differential level were based on perturbative methods. This probably obeys to the inherent complexity of these targets, which make difficult the implementation of numerical intensive methods, of great success in atoms and H_2 molecules [24–29], and only applied to heavier molecules under the approximation of a one-electron treatment [30]. The most implemented models to study the single ionization of molecules by electron impact are the DWBA [31] and its variations [32–37], while variants of the Born-3C method were applied to a lesser extent [38,39]. These perturbative methods achieved more than acceptable results for the targets under consideration throughout several decades.

In a previous work, we implemented the CDW-EIS approximation to study the single ionization of H_2O by electron impact at 81 eV, and found good overall agreement with the experimental data from Ref. [15], concluding that the inclusion of the asymptotic Coulomb distortion through eikonal phases in the initial state improves the description of this collision process at such impact energy [40]. This

[*]Contact author: emiliano.acebal@uns.edu.ar
[†]Contact author: sotranto@uns.edu.ar

theoretical method, widely used with great success in ion-atom [41–51] and ion-H_2O collisions [52–54], was scarcely implemented in the context of electron projectiles and atomic targets [40,55–59]. More recently, we have introduced a multicenter CDW-EIS description to analyze oriented H_2 targets, and obtained very good agreement with the experimental data for symmetric kinematic conditions [60]. However, its implementation for nonoriented complex molecules still represents a challenge, mainly due to the computational cost involved compared to the single-center approach.

In this work, we implement and analyze the capabilities and limitations of two single-center approximations to describe the interactions of the continuum electrons with the molecular ion. Under the framework of the CDW-EIS approximation we study the single ionization of the $1b_1$ and $3a_1$ molecular orbitals of H_2O and the $9b$ and $12a'$ molecular orbitals of the C_2 and C_s conformers of THF, respectively, by electron impact at intermediate to low impact energies. We benchmark our results with recent experimental data and the reported theoretical data obtained by two state-of-the-art theoretical models.

In the next section we describe the theoretical model. Results are discussed in Sec. III, and the conclusions and outlook are drawn in Sec. IV. Atomic units are used throughout this work unless otherwise stated.

II. THEORETICAL MODEL

The TDCS for the electron-impact ionization of a molecule and for a particular orientation of the molecular axes defined by the set of Euler angles (α, β, γ) is given by

$$\frac{d^6\sigma}{dE d\Omega_1 d\Omega_2 d\alpha d\beta d\gamma} = N_e (2\pi)^4 \frac{k_1 k_2}{k_0} \times \left[\frac{1}{4}\left|T_{fi}^D + T_{fi}^E\right|^2 + \frac{3}{4}\left|T_{fi}^D - T_{fi}^E\right|^2\right]. \tag{1}$$

Here, $N_e = 2$ represents the number of identical electrons in the molecular orbital to be ionized, $k_1 = \|\mathbf{k}_1\| = \sqrt{2E_1}$ and $k_2 = \|\mathbf{k}_2\| = \sqrt{2E_2}$ are the scattered projectile and emitted electron final momenta, respectively, E_1 and E_2 being their emission energies, and $k_0 = \|\mathbf{k}_0\| = \sqrt{2E_0}$ is the impinging projectile momentum, being E_0 the projectile impact energy. T_{fi}^D and T_{fi}^E are the direct and exchange transition amplitudes, with $T_{fi}^E(\mathbf{k}_1, \mathbf{k}_2) = T_{fi}^D(\mathbf{k}_2, \mathbf{k}_1)$. The capture channel is neglected in our one-active-electron theoretical treatment and therefore is not included in Eq. (1).

The Gellman-Goldberger amplitude T_{fi} in Eq. (1) is represented in its post version by

$$T_{fi} = \langle \Psi_f^- | W_f | \Psi_i^+ - \psi_i \rangle + \langle \Psi_f^- | V_i | \psi_i \rangle. \tag{2}$$

Here, ψ_i is the Born initial state

$$\psi_i = \frac{e^{i\mathbf{k}_0\cdot\mathbf{r}_1}}{(2\pi)^{3/2}} \varphi_i(\mathbf{r}_2), \tag{3}$$

and Ψ_i^+ is the eikonal initial state (EIS)

$$\Psi_i^+ = \frac{e^{i\mathbf{k}_0\cdot\mathbf{r}_1}}{(2\pi)^{3/2}} \varepsilon(\mathbf{r}_1)\varepsilon(\mathbf{r}_{12})\varphi_i(\mathbf{r}_2), \tag{4}$$

where $\varepsilon(\mathbf{r}_1)$ and $\varepsilon(\mathbf{r}_{12})$ are the eikonal phases

$$\varepsilon(\mathbf{r}_1) = e^{-\frac{iZ}{k_0}\ln(k_0 r_1 - \mathbf{k}_0\cdot\mathbf{r}_1)}, \qquad \varepsilon(\mathbf{r}_{12}) = e^{\frac{i}{k_0}\ln(k_0 r_{12} - \mathbf{k}_0\cdot\mathbf{r}_{12})}, \tag{5}$$

which are asymptotic solutions to the two-body Coulomb problem between the projectile and a single center of charge $Z = 1$ and the active electron, respectively, as described in previous works [40,60]. We define $\mathbf{r}_1$ and $\mathbf{r}_2$ as the positions of the projectile and the active electron, respectively, and $r_{12} = \|\mathbf{r}_{12}\| = \|\mathbf{r}_1 - \mathbf{r}_2\|$.

The wave function $\varphi_i(\mathbf{r}_2)$ describes the molecular orbital of the target. For H_2O, we make use of Moccia's self-consistent-field one-center-expanded molecular orbitals [61]:

$$\varphi_i^{H_2O}(\mathbf{r}_2) = \sum_{j=1}^{N_i} a_{ij} R_{n_{ij}}^{\xi_{ij}}(r_2) H_{l_{ij}}^{m_{ij}}(\hat{\mathbf{r}}_2), \tag{6}$$

where $H_{l_{ij}}^{m_{ij}}$ are the real spherical harmonics and $R_{n_{ij}}^{\xi_{ij}}$ are Slater type functions centered on the oxygen atom given by

$$R_{n_{ij}}^{\xi_{ij}}(r_2) = \sqrt{\frac{(2\xi)^{2n_{ij}+1}}{(2n_{ij})!}} e^{-\xi_{ij} r_2} r_2^{n_{ij}-1}. \tag{7}$$

The real spherical harmonics $H_{l_{ij}}^{m_{ij}}$ can be written as a function of the complex spherical harmonics $Y_{l_{ij}}^{m_{ij}}$ as follows:

$$H_{l_{ij}}^{m_{ij}} = \begin{cases} \frac{1}{\sqrt{2}}\left(Y_{l_{ij}}^{m_{ij}} + (-1)^{m_{ij}} Y_{l_{ij}}^{-m_{ij}}\right), & \text{if } m_{ij} > 0, \\ \frac{1}{i\sqrt{2}}\left(Y_{l_{ij}}^{|m_{ij}|} - (-1)^{|m_{ij}|} Y_{l_{ij}}^{-|m_{ij}|}\right), & \text{if } m_{ij} < 0, \\ Y_{l_{ij}}^{m_{ij}}, & \text{if } m_{ij} = 0. \end{cases} \tag{8}$$

In this sense, it is convenient to separate the radial and angular parts in Eq. (6):

$$\varphi_i^{H_2O}(\mathbf{r}_2) = \sum_{l_i m_i} \mathfrak{R}_{l_i}^{m_i}(r_2) b_i Y_{l_i}^{m_i}(\hat{\mathbf{r}}_2), \tag{9}$$

where the radial part $\mathfrak{R}_{l_i}^{m_i}$ is

$$\mathfrak{R}_{l_i}^{m_i}(r_2) = \sum_j a_{ij} R_{n_{ij}}^{\xi_{ij}}(r_2), \tag{10}$$

and b_i is a multiplicative factor arising from Eq. (8). The sum (10) is extended for all j that satisfy $l_{ij} = l_i$ and $m_{ij} = m_i$.

Regarding the C_4H_8O target, the molecular orbital wave function $\varphi_i(\mathbf{r}_2)$ was calculated by means of the linear combination of atomic orbitals (LCAO) approximation

$$\varphi_i^{C_4H_8O}(\mathbf{r}_2) = \sum_{j=1}^{N_{AO}} C_j \varphi'_j(\mathbf{r}_2). \tag{11}$$

In this expression, N_{AO} is the number of atomic orbitals $\varphi'_j(\mathbf{r}_2)$ used, which were expanded by means of the 6-31G basis set. The C_j coefficients for the molecular orbital were determined by a self-consistent field calculation performed by the GAMESS quantum chemistry package [62].

The initial perturbation operator V_i in Eq. (2) is written as

$$V_i = V_{\text{ion}}(\mathbf{r}_1) + \frac{1}{r_{12}}, \tag{12}$$

where the first term represents the projectile-ion attractive interaction, and the second one stands for the Coulomb repulsion between the projectile and the active electron.

The final state wave function represents two electrons in the continuum of the molecular ion and is given by

$$\Psi_f^- = \chi^-(\mathbf{k}_1, \mathbf{r}_1)\chi^-(\mathbf{k}_2, \mathbf{r}_2)\zeta(\mathbf{k}_{12}, \mathbf{r}_{12}), \tag{13}$$

where the postcollisional interaction (PCI) is represented by the confluent hypergeometric function

$$\zeta(\mathbf{k}_{12}, \mathbf{r}_{12}) = N^-(\alpha_3) \times {}_1F_1(i\alpha_3, 1, -ik_{12}r_{12} - i\mathbf{k}_{12}\cdot\mathbf{r}_{12}), \tag{14}$$

solution to the Coulomb potential between the pair of electrons. Here, $\mathbf{k}_{12} = (\mathbf{k}_1 - \mathbf{k}_2)/2$, $\alpha_3 = 1/(2k_{12})$ is the Sommerfeld parameter for the electron-electron interaction and $N^-(\alpha_3) = e^{-\alpha_3\pi/2}\Gamma(1 - i\alpha_3)$. The final perturbation operator W_f in Eq. (2) is obtained from the Schrödinger equation $(H - E)\Psi_f^- = W_f\Psi_f^-$ leading to

$$W_f = -\left(\frac{\nabla_{\mathbf{r}_1} f^-(\mathbf{k}_1, \mathbf{r}_1)}{f^-(\mathbf{k}_1, \mathbf{r}_1)}\right)\cdot\left(\frac{\nabla_{\mathbf{r}_{12}}\zeta(\mathbf{k}_{12}, \mathbf{r}_{12})}{\zeta(\mathbf{k}_{12}, \mathbf{r}_{12})}\right) + \left(\frac{\nabla_{\mathbf{r}_2} f^-(\mathbf{k}_2, \mathbf{r}_2)}{f^-(\mathbf{k}_2, \mathbf{r}_2)}\right)\cdot\left(\frac{\nabla_{\mathbf{r}_{12}}\zeta(\mathbf{k}_{12}, \mathbf{r}_{12})}{\zeta(\mathbf{k}_{12}, \mathbf{r}_{12})}\right), \tag{15}$$

being $f^-(\mathbf{k}_i, \mathbf{r}_i) = (2\pi)^{3/2}e^{-i\mathbf{k}_i\cdot\mathbf{r}_i}\chi^-(\mathbf{k}_i, \mathbf{r}_i)$, with $i = 1, 2$.

The distorted waves $\chi^-(\mathbf{k}_i, \mathbf{r}_i)$ take into account the interaction of the scattered projectile and the emitted electron with the molecular ionic core via the potential

$$V_{\text{ion}}(\mathbf{r}_i) = \overbrace{V^{e-N}(\mathbf{r}_i)}^{} + \overbrace{V^{e-e}(\mathbf{r}_i)}^{} = -\sum_{j=1}^{N}\frac{Z_j}{R_{ij}} + \sum_{n=1}^{N_{\text{MO}}} N_e \int d^3\mathbf{r}'\frac{|\varphi_n(\mathbf{r}')|^2}{|\mathbf{r}_i - \mathbf{r}'|}. \tag{16}$$

Here, the first sum V^{e-N} represents the particles interaction with the N nuclei of the molecule, where Z_j are the different atomic numbers corresponding to each nuclei and R_{ij} is the modulus of the vector $\mathbf{R}_{ij} = \mathbf{r}_i - \mathbf{R}_j$, being $\mathbf{R}_j$ the position of each nuclei. The second sum V^{e-e} stands for the particles interactions with the ion-remaining electrons. N_{MO} is the number of occupied molecular orbitals, $|\varphi_n(\mathbf{r}')|^2$ are the different electron densities corresponding to each orbital, and N_e is the number of electrons present in the nth orbital.

The simplest approximation to V_{ion} completely neglects the multicenter nature of the residual ion by considering it as a single center of charge $Z = 1$ [$V_{\text{ion}}(\mathbf{r}_i) \simeq V_{1C}(r_i) = -Z/r_i$]. In this case, the distorted waves $\chi^-(\mathbf{k}_i, \mathbf{r}_i)$ are just described by the Coulomb functions

$$C^-(\mathbf{k}_i, \mathbf{r}_i) = \frac{e^{i\mathbf{k}_i\cdot\mathbf{r}_i}}{(2\pi)^{3/2}}N^-(\alpha_i) \times {}_1F_1(i\alpha_i, 1, -ik_ir_i - i\mathbf{k}_i\cdot\mathbf{r}_i), \tag{17}$$

with $i = 1, 2$. This leads to the commonly known CDW or 3C final state, which was employed with success to describe the ionization of H_2O by electron impact in energetic asymmetrical conditions [38,40].

A second approximation consists in spherically averaging the anisotropic potential V_{ion} to obtain

$$U(r_i) = \frac{1}{4\pi}\int d\Omega\, V_{\text{ion}}(\mathbf{r}_i). \tag{18}$$

This average procedure provides an isotropic description of the molecular ion, the main advantage of which relies on the fact that the distorted waves $\chi^-(\mathbf{k}_i, \mathbf{r}_i)$ can be separated into a radial part and an angular part with respect to only one center,

$$\chi^-(\mathbf{k}_i, \mathbf{r}_i) = \sum_{l=0}^{\infty}\frac{(2l+1)}{k_ir_i}i^l e^{-i\sigma_l}u_l(k_i, r_i)P_l(\hat{k}_i\cdot\hat{r}_i). \tag{19}$$

Here, $\sigma_l = \sigma_l^{\text{Coul}} + \delta_l$, $\sigma_l^{\text{Coul}} = \arg[\Gamma(l + 1 + i\alpha_i)]$, δ_l is the non-Coulombic phase shift of the radial waves ($\delta_l = 0$ for the Coulomb radial waves) and $P_l(\hat{k}_i\cdot\hat{r}_i)$ are the Legendre polynomials. The radial wave functions $u_l(k_i, r_i)$ satisfy the equation

$$\left[-\frac{1}{2}\frac{d^2}{dr_i^2} + \frac{l(l+1)}{2r_i^2} + U(r_i)\right]u_l(k_i, r_i) = \frac{k_i^2}{2}u_l(k_i, r_i). \tag{20}$$

This approximation was employed in previous works on ion-CH_4 and ion-H_2O collisions, obtaining for the latter good overall agreement with reported experimental doubly differential cross sections [63,64]. For electron impact, a similar spherical average procedure was employed for NH_3, CH_4, and H_2O [65–68]. This procedure led to the satisfactory description of the experimental TDCS at the binary peak structure, but led to mixed results in the denominated recoil peak region.

The partial waves $u_l(k_i, r_i)$, together with the non-Coulombic phase shifts δ_l, can be obtained through Salvat's code [69]. These phase shifts become negligible as l increases, and due to the asymptotic limit of these potentials, the radial wave functions $u_l(k_i, r_i)$ converge to the Coulombic ones $u_l^{\text{Coul}}(k_i, r_i)$, which are solutions of Eq. (20) with potential $V_{1C}(r_i)$. Therefore, in our computer code, the distorted waves $\chi^-(\mathbf{k}_i, \mathbf{r}_i)$ are written as

$$\chi^-(\mathbf{k}_i, \mathbf{r}_i) = C^-(\mathbf{k}_i, \mathbf{r}_i) + \sum_{l=0}^{L}\frac{(2l+1)}{k_ir_i}i^l P_l(\hat{k}_i\cdot\hat{r}_i) \times \left(e^{-i\sigma_l}u_l(k_i, r_i) - e^{-i\sigma_l^{\text{Coul}}}u_l^{\text{Coul}}(k_i, r_i)\right). \tag{21}$$

By doing so, the infinite partial waves can be accounted for by correcting from the asymptotic Coulomb wave function the partial waves for l values lower than a certain L. The latter is determined by analyzing the L value from which the non-Coulombic phase shift δ_l can be considered negligible thus reaching convergence. This strategy considerably reduces the numerical effort to be performed. This model will be referred to as spherically averaged distorted waves (SADW) final state.

The calculation of the transition amplitude (T_{fi}) in Eq. (2) involves a six-dimensional integration which was directly performed by the adaptive Vegas Monte Carlo algorithm [70]. The wave-packet approach of Malcherek and Briggs [71] was used, in order to treat the continuum-continuum transition. We estimate our numerical uncertainty to be less than 5%.

In order to compare our calculations with the experimental data it is necessary to perform an average procedure by

evaluating the integral

$$\frac{d^3\sigma}{dEd\Omega_1 d\Omega_2} = \frac{1}{8\pi^2}\int_0^{2\pi}\int_0^{\pi}\int_0^{2\pi}\frac{d^6\sigma}{dEd\Omega_1 d\Omega_2 d\alpha d\beta d\gamma} \times \sin\beta d\alpha d\beta d\gamma, \quad (22)$$

over the three Euler angles α, β, and γ, since the experimental data do not resolve the orientation of the target at the collision instant.

For the ionization of H_2O, this procedure can be done analytically, given that their molecular orbitals $\varphi_i(\mathbf{r}_2)$ in Eq. (9) are one-center expanded. Therefore, they can be expressed as an explicit function of the Euler angles

$$\varphi_i^{H_2O}(\mathbf{r}_2) = \sum_{l_i m_i}\sum_{\mu=-l_i}^{l_i}\mathfrak{R}_{l_i}^{m_i}(r_2) b_i D_{\mu m_i}^{(l_i)}(\alpha,\beta,\gamma) Y_{l_i}^{\mu}(\hat{\mathbf{r}}_2). \quad (23)$$

Here $D_{\mu m_i}^{(l_i)}(\alpha,\beta,\gamma)$ is the finite rotation matrix given by

$$D_{\mu m_i}^{(l_i)}(\alpha,\beta,\gamma) = e^{i\mu\gamma} d_{\mu m_i}^{(l_i)}(\beta) e^{i m_i \alpha}, \quad (24)$$

and the functions $d_{\mu m_i}^{(l_i)}(\beta)$ are defined through Jacobi polynomials [72,73]. In this sense, the transition amplitude (T_{fi}) for a particular orientation of the molecular axes can be written as

$$T_{fi} = \sum_{l_i m_i}\sum_{\mu=-l_i}^{l_i} b_i D_{\mu m_i}^{(l_i)}(\alpha,\beta,\gamma) S_{l_i m_i}^{\mu}, \quad (25)$$

where $S_{l_i m_i}^{\mu}$ is defined as Eq. (2) with

$$\varphi_i(\mathbf{r}_2) = \mathfrak{R}_{l_i}^{m_i}(r_2) Y_{l_i}^{\mu}(\hat{\mathbf{r}}_2). \quad (26)$$

Finally, we can use the orthogonality relation

$$\frac{1}{8\pi^2}\int_0^{2\pi}\int_0^{\pi}\int_0^{2\pi} D_{\mu m}^{(l)}(\alpha,\beta,\gamma) D_{\mu' m'}^{(l')*}(\alpha,\beta,\gamma) \times \sin\beta d\alpha d\beta d\gamma = \frac{1}{2l+1}\delta_{ll'}\delta_{mm'}\delta_{\mu\mu'} \quad (27)$$

to analytically evaluate the integral of Eq. (22) and obtain the averaged TDCS

$$\frac{d^3\sigma}{dEd\Omega_1 d\Omega_2} = N_e (2\pi)^4 \frac{k_1 k_2}{k_0}\sum_{l_i m_i}\sum_{\mu=-l_i}^{l_i}\frac{1}{2l_i+1}\left|S_{l_i m_i}^{\mu}\right|^2. \quad (28)$$

Consequently, the computational effort to calculate the averaged TDCS for the ionization of H_2O is considerably reduced. It requires the computation of only 22 and 28 different $S_{l_i m_i}^{\mu}$ integrals for the $1b_1$ and $3a_1$ orbitals of H_2O, respectively [61]. On the other hand, each term of the molecular orbital wave function of THF in Eq. (11) is expanded over different atomic centers. It should be pointed out that numerical monocentric wave functions can be obtained from Eq. (11) by performing a single-center expansion [74–76]. Nevertheless, while in principle this could allow an analytic evaluation of Eq. (22) for the THF molecule, in our work the number of $S_{l_i m_i}^{\mu}$ integrals to be calculated exceeds the number of transition amplitudes T_{fi} required to converge the numerical average procedure. In this work, the extended Simpson's rule with numerical steps of $\Delta\alpha = 30^\circ$, $\Delta\beta = 15^\circ$, and $\Delta\gamma = 30^\circ$ was employed, after punctual checks of convergence using a denser mesh. This accounts for calculating 1584 different transition amplitudes T_{fi}, for each molecular orbital of each conformer of THF. It then becomes evident that benchmarking theoretical models with experimental data regarding nonoriented molecular targets, is much more time consuming in computational terms, when the initial state molecular orbitals are not single-center expanded, even when the single-center approach for the molecular ion is used in its final state.

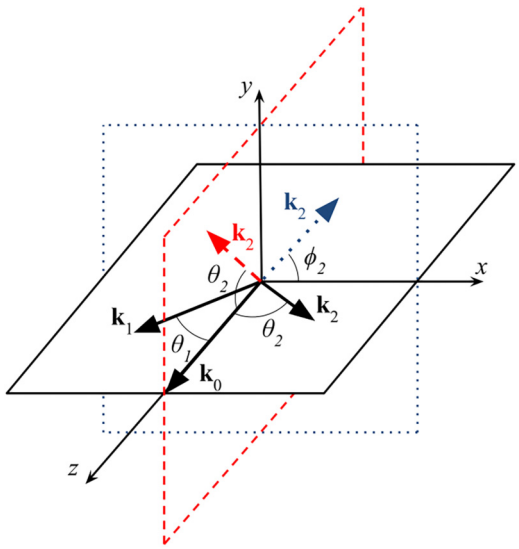

FIG. 1. Electron emission planes considered in this work: the scattering plane xz (solid frame), the perpendicular plane yz (dashed frame), and the full-perpendicular plane xy (dotted frame). The angles θ_1, θ_2, and ϕ_2 were taken as positive counterclockwise.

III. RESULTS

In this section we present the calculated TDCS for the electron-impact single ionization of H_2O and THF by means of the two single-center models introduced in the previous section: the CDW-EIS and the SADW-EIS.

Present results are benchmarked against recent experimental data, and the predictions of the M3DW and MCTDW theoretical models. The M3DW approximation mainly differs from the SADW-EIS in the initial state description. The former approximates the projectile-target interaction with a neutral potential [31,37], whereas the eikonal initial state asymptotically solves the Coulomb interactions with the active electron and molecular ion separately. In contrast, the MCTDW method describes the interaction with the molecular ion through multicenter distorted waves, using an anisotropic potential [34–36]. The PCI effect is exactly included in the CDW-EIS, SADW-EIS, and M3DW models, while in the MCTDW approximation it is introduced via the Ward-Macek method [77].

Three different emission planes are analyzed: the scattering plane xz, defined by the initial and final momenta of the projectile $\mathbf{k}_0$ and $\mathbf{k}_1$, the perpendicular plane yz, which is the perpendicular plane to the scattering plane that contains the impinging momentum $\mathbf{k}_0$, and the full-perpendicular plane xy, perpendicular to $\mathbf{k}_0$. These are presented in Fig. 1.

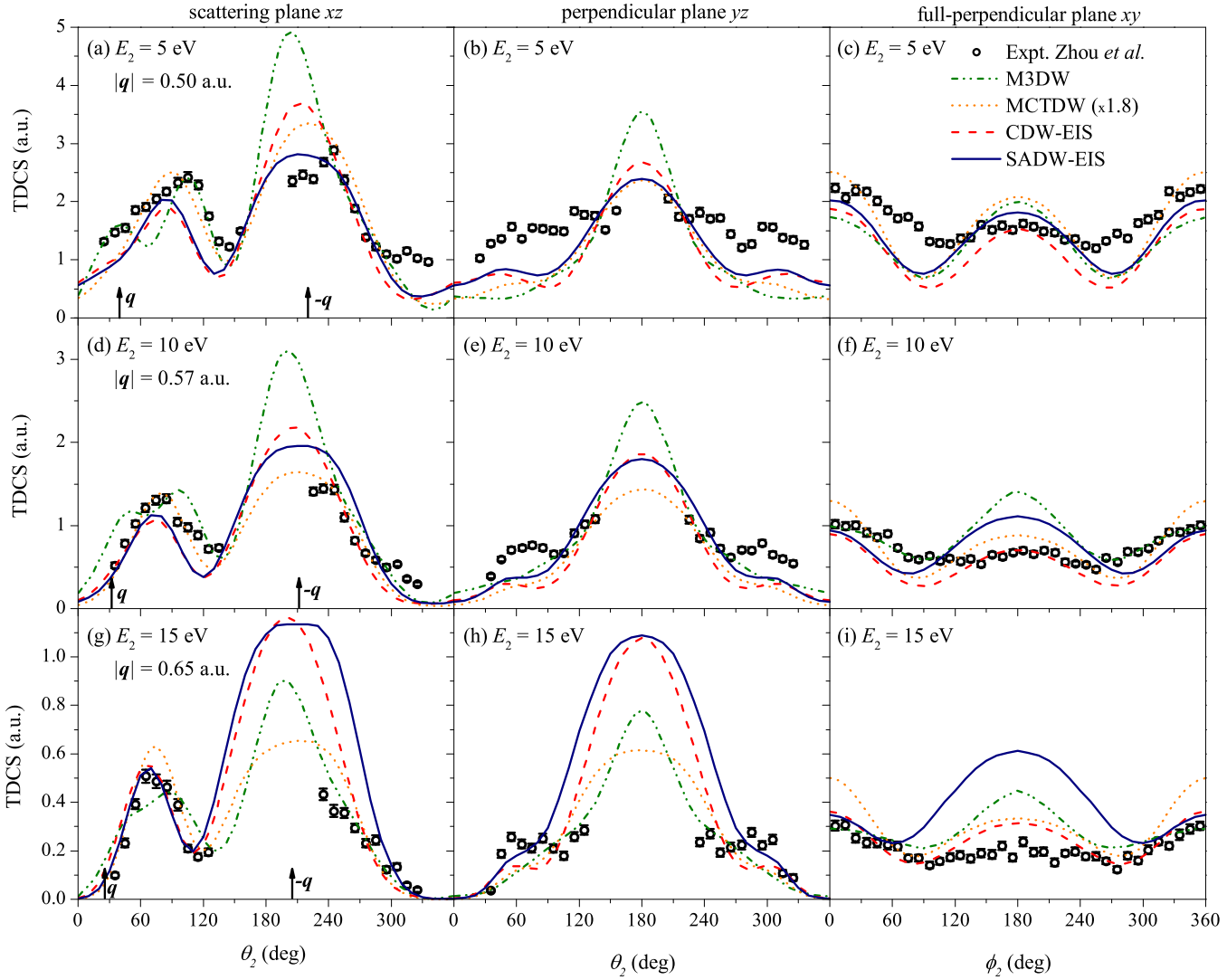

FIG. 2. TDCS for the single ionization of H_2O by 65 eV electron impact, calculated by means of the CDW-EIS and SADW-EIS models, as a function of the emitted electron angle in the scattering plane xz (left column), perpendicular plane yz (center column), and full-perpendicular plane xy (right column), for an emitted electron energy of 5 eV (top row), 10 eV (center row), and 15 eV (bottom row), and a projectile scattering angle of $-10°$. Experimental data and theoretical results for M3DW and MCTDW methods were obtained from Ref. [16].

A. Single ionization of H_2O

The TDCS for the single ionization of H_2O by electron impact were calculated at an impact energy of 65 eV. As stated in the experimental work [16], ionization from the $1b_1$ and $3a_1$ orbitals leading to the H_2O^+ cation was studied. Due to the limited binding energy resolution, these orbitals could not be resolved. As a result, the reported data correspond to the summed TDCS of the $1b_1$ and $3a_1$ orbitals. In addition, the absolute value of the TDCS was determined in the measurements, thus providing a stringent test for the theoretical models. The final kinematic conditions are $E_2 = 5$ eV, 10 eV, and 15 eV for the emitted electron energy and $\theta_1 = -10°$ and $-15°$ for the projectile scattering angle. In Eq. (21) convergence was reached for $L = 3$, 3, and 4 for the emitted electron and $L = 7$, 7, and 6 for the projectile, for $E_2 = 5$ eV, 10 eV, and 15 eV, respectively.

In the first place, in Fig. 2, we present the TDCS for a projectile scattering angle of $\theta_1 = -10°$. In the left column we analyze the emission into the scattering plane, defined by the initial and final momenta of the projectile $\mathbf{k}_0$ and $\mathbf{k}_1$ [Figs. 2(a), 2(d), and 2(g)]. It can be seen that the experimental data exhibit a well-known structure consisting of two peaks: the binary peak at lower emission angles, which can be classically interpreted as a single collision of the active electron with the projectile, and the recoil peak at higher emission angles, which can be interpreted as resulting from a secondary collision of the emitted electron with the remaining ion. We observe that the CDW-EIS and SADW-EIS models fail to predict the position and magnitude of the binary peak at the lower emission energy considered of 5 eV. Increasing this energy to 10 eV, the description of the experimental binary structure improves, and for 15 eV, these models are in very good agreement with the experimental data. Besides, we observe that they predict a similar binary structure, since they differ in the description of the final state of the collision, therefore expecting that the differences between them arise in the recoil region.

Regarding the description of the recoil peak, we observe that for $E_2 = 5$ eV, in Fig. 2(a), the CDW-EIS model overestimates the experimental structure, while the SADW-EIS predicts the correct magnitude. As the emission energy increases to 15 eV [Fig. 2(g)], both models lead to similar results and tend to overestimate the experimental recoil peak intensity. The magnitude of the momentum transfer vector $\mathbf{q} = \mathbf{k}_0 - \mathbf{k}_1$, for electron emission energies of 5 eV and 10 eV, is 0.50 a.u. and 0.57 a.u., respectively. It is worth mentioning that these values of $|\mathbf{q}|$ are the average of the ones obtained from ionization of the $1b_1$ and $3a_1$ molecular orbitals. These magnitudes were already considered in our previous work at an impact energy of 81 eV [40]. However, for $E_2 = 15$ eV, the electron momentum magnitude equals 1.05 a.u. while the modulus of $\mathbf{q}$ is equal to 0.65 a.u.. This implies an increasing role of momentum exchange between the molecular ion and the emitted electron compared to the other geometries. These trends suggest that geometries associated to electron emission with momentum magnitudes much higher than the projectile momentum transfer could be particularly useful to test the final state models currently used.

In comparison with the other theoretical methods, we observe that the M3DW approximation predicts a two-peak binary structure, not exhibited by the experimental data, indicating that the asymptotic Coulomb distortion in the initial channel provides a better agreement of this collision process, as was concluded at an impact energy of 81 eV [40]. In addition, this approximation overestimates the recoil peak for the three emission energies considered. In contrast, the MCTDW model correctly reproduces the binary structure for low emission energies and is in better agreement with the experimental data than the other methods in the recoil region for $E_2 = 10$ eV and 15 eV. This suggests that, at an impact energy of 65 eV, the multicenter effects of the molecular ion are more significant. Nevertheless, and bearing in mind that the absolute magnitude of the experimental data was measured, it should be pointed out the MCTDW results underestimates this magnitude by a factor of 1.8, whereas the other theoretical methods predict the correct TDCS magnitude at the binary peak.

Secondly, in Figs. 2(b), 2(e), and 2(h), we analyze emission into the perpendicular plane yz, which is the perpendicular plane to the scattering plane that contains the impinging momentum $\mathbf{k}_0$. It can be observed that the experimental data are symmetric with respect to the beam direction ($\theta_2 = 180°$), and three peaks are exhibited, with two maxima around $\theta_2 \simeq 60°$ and $\theta_2 \simeq 300°$, which represent a binary collision with the projectile, and a third peak at $\theta_2 = 180°$, which can be interpreted as a double scattering of the emitted electron, first with the projectile and then with the molecular ion. This owes to the fact that this emission plane intersects the scattering plane xz at $\theta_2 = 0°$ and $\theta_2 = 180°$, which corresponds to the same θ_2 values in the scattering plane (see Fig. 1).

For an emission energy of 5 eV, in Fig. 2(b), we observe that the CDW-EIS and SADW-EIS models are in agreement with the three-peak experimental structure, predicting the correct position of the maxima, and that the latter slightly improves the description of their relative magnitudes. However, both methods underestimate the binary region. Increasing the emitted electron energy to 10 eV and 15 eV, in Figs. 2(e) and 2(h), respectively, we again observe an improvement in the description of the binary maxima and an overestimation of the central recoil peak at $\theta_2 = 180°$. For this emission plane, the SADW-EIS provides a better description of the experimental data in the binary region, while a more quantitative analysis at the recoil peak is not allowed, due to the unavailability of experimental data along the incident beam direction.

In order to complete the analysis for $\theta_1 = -10°$, in Figs. 2(c), 2(f), and 2(i), we analyze the electron emission into the full-perpendicular plane xy, defined as the plane perpendicular to $\mathbf{k}_0$. In this case, the experimental data are symmetric with respect to $\phi_2 = 180°$, and exhibit a two-peak structure, with a binary region around $\phi_2 = 0°$ and a recoil peak at $\phi_2 = 180°$. Once again, we observe an underestimation of the binary region by the CDW-EIS and SADW-EIS models, except for $E_2 = 15$ eV. Interestingly, for this emission plane, the CDW-EIS method is in better agreement with the experimental data than the SADW-EIS in the recoil region, for the three emission energies considered. It is worth mentioning that this emission plane intersects the scattering plane xz at $\phi_2 = 0°$ and $\phi_2 = 180°$, which corresponds to values of $\theta_2 = 90°$ and $\theta_2 = 270°$ in the scattering plane, respectively (see Fig. 1). Therefore, the higher magnitude predicted by the SADW-EIS model at $\phi_2 = 180°$ in Figs. 2(c), 2(f), and 2(i) is related to the wider recoil structure exhibited by this method in the scattering plane in Figs. 2(a), 2(d), and 2(g). In addition, it is surprising that the CDW-EIS seems to be the theoretical method that best reproduces the experimental data for this emission plane, for the three emission energies considered, except for the binary structure in Fig. 2(f), where the M3DW approximation is in excellent agreement with the experiment.

Figure 3 shows the TDCS results for a projectile scattering angle of $\theta_1 = -15°$. Considering the electron emission into the scattering plane, in Figs. 3(a), 3(d), and 3(g), we observe that the TDCS are similar to the ones presented for $\theta_1 = -10°$ in Fig. 2 and it can be seen that the CDW-EIS and the SADW-EIS models are the ones that exhibit the best agreement with the experimental binary peak structure for the three emission energies considered. This suggests that for large momentum transfers, the inclusion of the asymptotic Coulomb distortion in the initial channel becomes more important. On the other hand, the recoil structures for $E_2 = 10$ eV and 15 eV are still overestimated by these methods, while for $E_2 = 5$ eV the SADW-EIS is in very good agreement with the experiment.

In addition, it is worth mentioning that for $E_2 = 5$ eV, in Fig. 3(a), the experimental data suggest a two-peak binary structure, which is reproduced by the CDW-EIS and SADW-EIS models, and is not observed for the other kinematic conditions. For Ar(3p) targets, a CDW-EIS study in which TDCS were analyzed as a function of the projectile momentum transfer showed that the single-peak binary structure evolved into a two-peak structure, usually associated to p-type orbitals, as the projectile momentum transfer was increased [57]. Here, this two-peak structure only manifests for $E_2 = 5$ eV and seems to appear as the angle between the incident beam direction $\theta_2 = 0°$ and the momentum transfer direction $\mathbf{q}$ ($\theta_\mathbf{q}$) increases. Besides, an additional maximum around $\theta_2 = 300°$ shows up, which is not predicted by any of the theories. A more detailed study, analyzing the emergence of this additional peak and the evolution of the binary

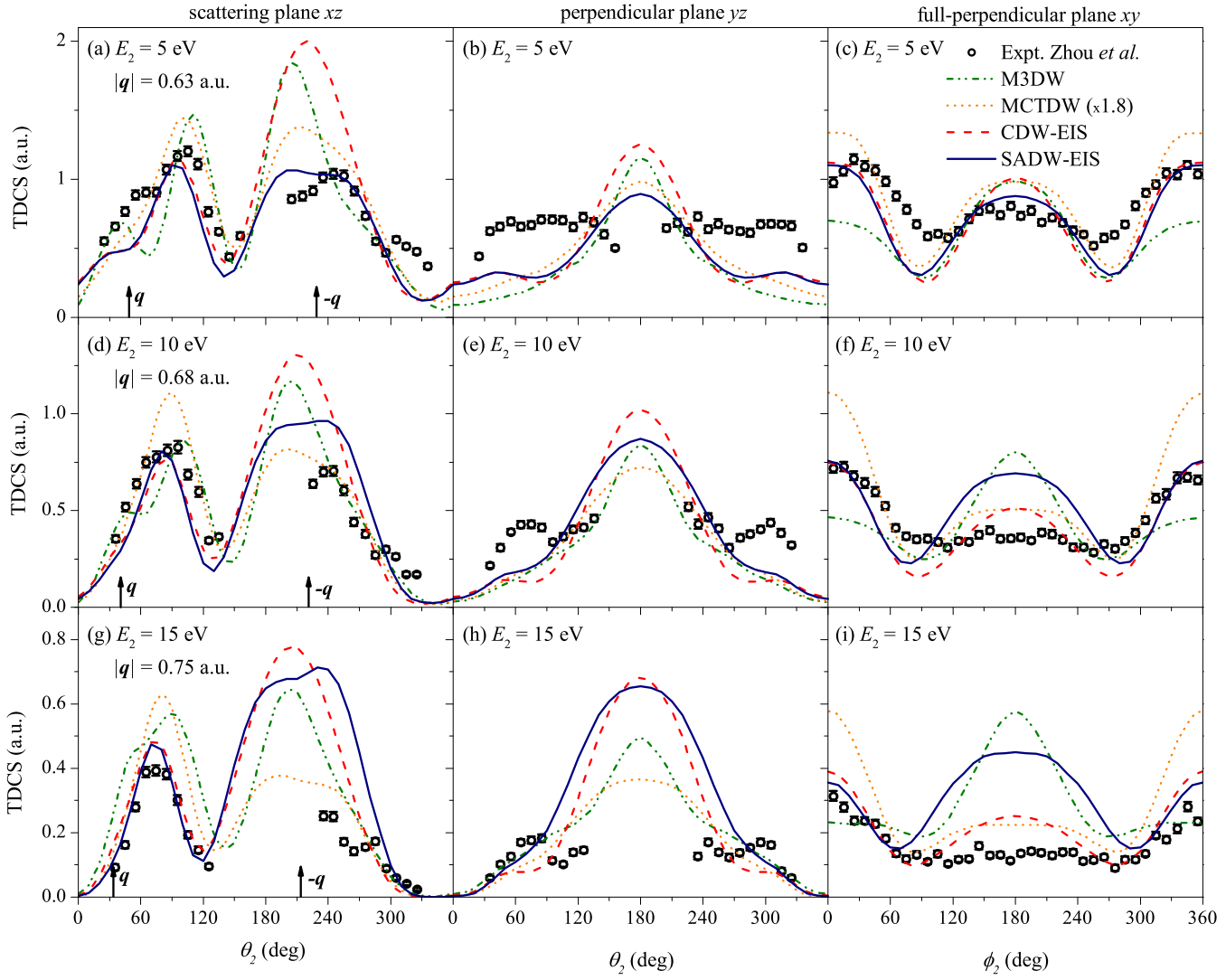

FIG. 3. Same as Fig. 2, but for a projectile scattering angle of $-15°$.

structure is suggested, increasing the spectrum of kinematic conditions.

Considering emission into the perpendicular plane yz, in Figs. 3(b), 3(e), and 3(h), we observe that the three-peak experimental structure is well reproduced by the CDW-EIS and SADW-EIS models, with an underestimation of the binary region for low emission energies, and an overestimation of the recoil region for high emission energies, already seen for $\theta_1 = -10°$ in Fig. 2. Once again, the SADW-EIS method provides the best agreement with the experimental binary structure.

Finally, for an electron emitted in the full-perpendicular plane xy, in Figs. 3(c), 3(f), and 3(i), we again observe that the CDW-EIS model is the one in best agreement with the experimental data, as was seen for $\theta_1 = -10°$ in Fig. 2, which is surprising since it is the theoretical method that includes, in the final state of the collision, the simplest description of the molecular ion.

In this sense, and to analyze in more detail the statements above included, in Fig. 4 we present the ratio between the recoil and binary peak of the full-perpendicular plane xy, *i. e.*, the TDCS at $\phi_2 = 180°$ divided by the TDCS at $\phi_2 = 0°$, with θ_2 fixed at 90°, as a function of the emitted electron energy. We include results obtained for projectile scattering angles of $-10°$, $-15°$, and $-20°$. From the analysis of Figure 4, we observe that the experimental ratio decreases as the emission energy increases, and it can be seen that the CDW-EIS and MCTDW models are in good agreement with the experimental data. This behavior, already observed in previous measurements at an impact energy of 81 eV [15], is expected, since for larger emission energies the active electron has less time to interact with the molecular ion, and therefore, the probability of backward emission ($\phi_2 = 180°$) is disfavored against forward emission ($\phi_2 = 0°$). On the other hand, the SADW-EIS and M3DW approximations predict a ratio that increases with the emission energy in disagreement with the experimental data of Fig. 4.

In addition, in Fig. 5 we present the same results, but as a function of the magnitude of the momentum transfer **q**, where we observe that the CDW-EIS and MCTDW models follow the experimental trends, as was observed in Fig. 4. On the other hand, it is striking that for $E_2 = 5$ eV, the SADW-EIS method correctly reproduces the recoil-binary ratio, except for the least momentum transfer case ($q = 0.50$ a.u.), where a slight overestimation is obtained. This emission energy

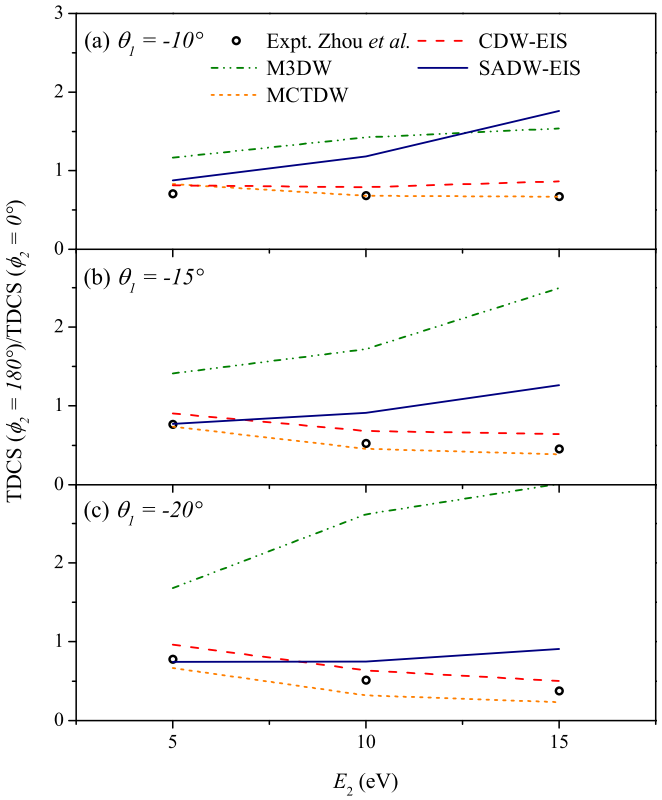

FIG. 4. TDCS recoil-binary ratio for the full-perpendicular plane xy, calculated by means of the CDW-EIS and SADW-EIS models, as a function of the emitted electron energy and for a projectile scattering angle of (a) $-10°$, (b) $-15°$, and (c) $-20°$. Experimental data and theoretical results for M3DW and MCTDW methods were obtained from Ref. [16].

corresponds to a final momentum magnitude of the active electron of $k_2 = 0.61$ a.u. Therefore, for the two cases where $q > k_2$, the SADW-EIS model is in very good agreement with the experimental recoil to binary ratio in the full-perpendicular plane. This inequality ($q > k_2$) implies that the

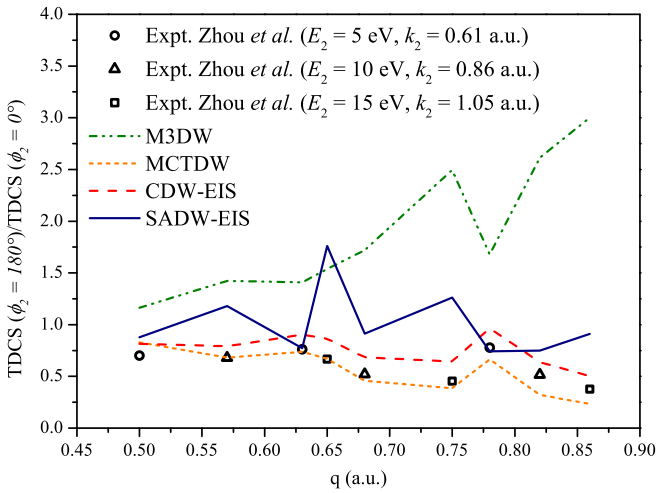

FIG. 5. Same as Fig. 4, but as a function of the magnitude of the projectile momentum transfer vector.

active electron can be emitted from a binary collision with the projectile, without the necessity of the molecular ion to participate. In this case, an overestimation of the interaction with the residual ion would not strongly affect the TDCS. In Figs. 2 and 3 we observed that the best agreement with the experimental data achieved by the SADW-EIS model was for $E_2 = 5$ eV and $\theta_1 = -15°$ [Figs. 3(a), 3(b), and 3(c)]. Besides, in Fig. 5, it can be seen that whenever $q < k_2$, the SADW-EIS model predicts a relative recoil-binary magnitude much higher than the experiment, with this difference becoming less significant as the magnitude of the momentum transfer q approaches the magnitude of the final momentum of the emitted electron k_2.

We can then conclude that a spherical average of the anisotropic potential of the H_2O^+ ion does not solve the discrepancies observed for every kinematic condition analyzed, with respect to approximating the molecular ion as a single center of charge $Z = 1$. Although a better description of the experimental data for the scattering and perpendicular planes is obtained by the SADW-EIS method, the CDW-EIS model predicts better results for the full-perpendicular plane at an impact energy of 65 eV.

B. Single ionization of THF

In order to extend the monocentric descriptions of the final state of the process of single ionization of molecules to more complex targets, in Fig. 6 we present the TDCS for the single ionization of THF by electron-impact calculated at an impact energy of 250 eV. This energy is much larger than the one considered for H_2O, and allows us to neglect the exchange transition amplitude in Eq. (1), thus reducing the computational cost by one-half. We benchmark our results with experimental data that represents emission from the $9b$ and $12a'$ molecular orbitals of the C_2 and C_s conformers of THF, respectively, in a 80% : 20% proportion [23] and with the theoretical models MCTDW and M3DW. Provided that the experimental data are relative, a common factor is used to normalize the results of Ref. [23], both experimental and theoretical, to our theoretical results. The final kinematic conditions are $E_2 = 10$ eV and 15 eV for the emitted electron energy and $\theta_1 = -10°$ for the projectile scattering angle. In Eq. (21) convergence was reached for $L = 7$ and $L = 8$ for the emitted electron and $L = 30$ and $L = 29$ for the projectile, for $E_2 = 10$ eV and $E_2 = 15$ eV, respectively.

First, in Figs. 6(a) and 6(d), we focus on electron emission into the scattering plane xz, where we observe that the experimental binary and recoil structures are not so well defined as for the H_2O case, mainly for $E_2 = 10$ eV. In addition, the binary region seems to exhibit a minimum around the direction of the momentum transfer $\mathbf{q}$, observed for H_2O when $\theta_\mathbf{q} > 40°$, in Fig. 3(a). In this case, for the kinematic conditions analyzed, $\theta_\mathbf{q} \simeq 70°$. It can be seen that the CDW-EIS and SADW-EIS models predict a double peak binary structure, reproducing the minimum around $\mathbf{q}$. In particular, the contributions to the molecular orbital $9b$ of the C_2 conformer are mostly from atomic orbitals of the p type. Nevertheless, the experimental structure seems to exhibit more than two peaks, feature that becomes less pronounced as the emission energy is increased from 10 eV to 15 eV. Regarding the recoil

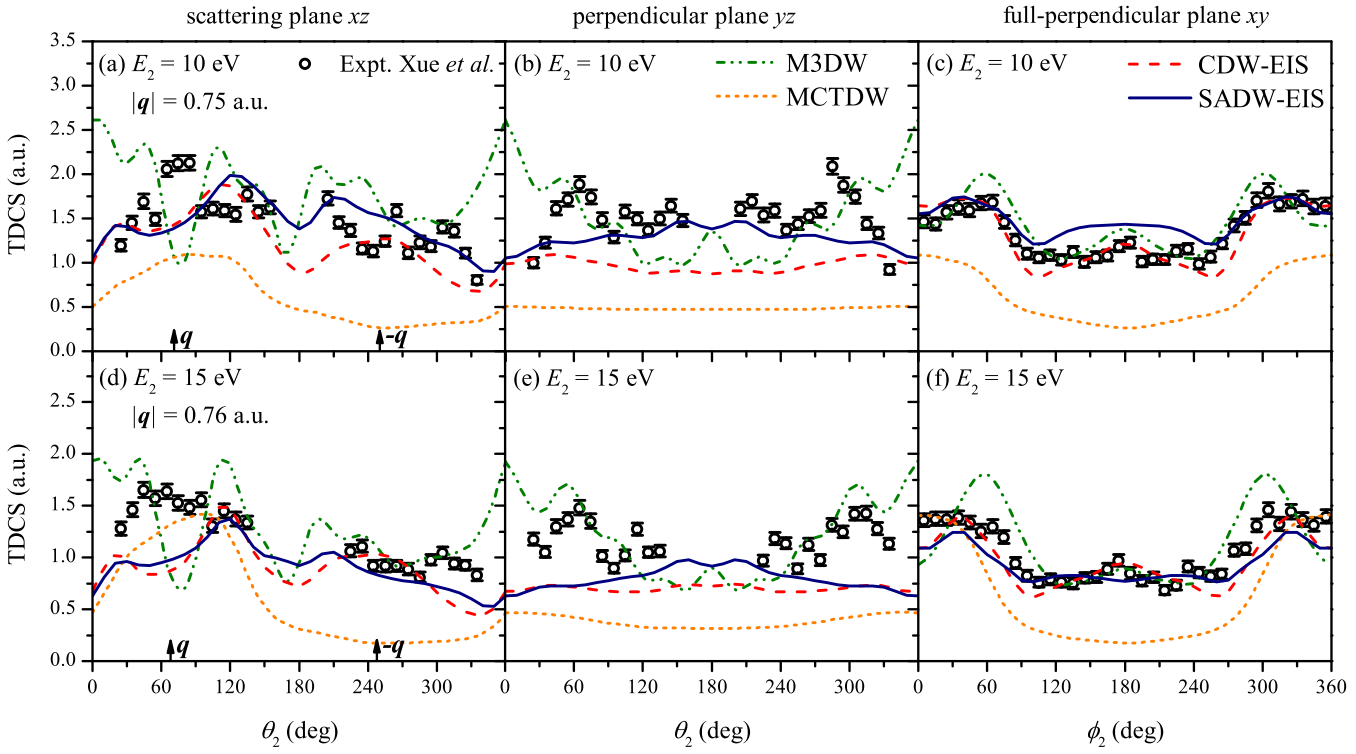

FIG. 6. TDCS for the single ionization of THF by 250 eV electron impact, calculated by means of the CDW-EIS and SADW-EIS models, as a function of the emitted electron angle in the scattering plane xz (left column), perpendicular plane yz (center column), and full-perpendicular plane xy (right column), for an emitted electron energy of 10 eV (top row) and 15 eV (bottom row), and a projectile scattering angle of $-10°$. Experimental data and theoretical results for M3DW and MCTDW methods from Ref. [23] were scaled to the present theoretical results.

structure, we observe that the SADW-EIS model improves the description of its relative magnitude, with respect to the binary region, mainly for an emitted electron energy of 10 eV. Besides, the CDW-EIS method predicts a unique recoil peak around the opposite direction of the momentum transfer, while the SADW-EIS suggests a structure consisting of a series of local maxima, with decreasing magnitude towards higher emission angles. This structure seems to better describe the experimental data.

From the comparison with the other theoretical methods, we observe that the M3DW approximation predicts an oscillatory structure throughout the whole angular range, correctly describing the relative magnitude between the recoil and binary regions, though exhibiting a maximum around the projectile scattering angle, in disagreement with the experiment. Moreover, the minimum predicted around **q** is much deeper than the one exhibited by the experimental data. On the other hand, the MCTDW model predicts a wide binary structure, which seems to properly describe the experimental data for $E_2 = 15$ eV, but with almost no recoil probability for any of the emission energies analyzed.

Figures 6(b) and 6(e) show the TDCS for emission into the perpendicular plane yz. There, we observe that the symmetry required by the cross section with respect to $\theta_2 = 180°$ is fulfilled by the experiment and the theories. The experimental data exhibit two maxima around $\theta_2 \simeq 60°$ and $\theta_2 \simeq 300°$, which are not reproduced by the CDW-EIS and SADW-EIS models. The former predicts a plane structure in the whole angular range, while the latter correctly describes the succession of local maxima exhibited by the experiment between $\theta_2 = 90°$ and $\theta_2 = 270°$, mainly for 10 eV. In contrast, the M3DW approximation reproduces the binary symmetric maxima, but predicts a peak around $\theta_2 = 0°$, not present in the experiment, as in the scattering plane. The MCTDW model presents no visible structure in the whole angular range for emission into the perpendicular plane yz.

Finally, considering emission into the full-perpendicular plane xy, in Figs. 6(c) and 6(f), we again observe that the symmetry around $\phi_2 = 180°$ is fulfilled by the experiment and the theoretical models. The experimental data show a three-peak structure, with a maximum around $\phi_2 = 180°$, corresponding to the recoil region, and two binary maxima around $\phi_2 \simeq 60°$ and $\phi_2 \simeq 300°$ for 10 eV, which become wider as the emission energy is increased to 15 eV. It can be seen that the CDW-EIS and SADW-EIS models correctly reproduce this structure, but with the latter not giving a recoil-binary ratio prediction as good as the former, as was observed for H_2O. In this case, the magnitude of the momentum transfer is lower than the final momentum of the emitted electron, for both emission energies considered. Nevertheless, the differences exhibited between these models in Figs. 6(c) and 6(f) are not big enough to attribute them to an overestimation of the interaction with the residual ion. In comparison with the other theories, we observe that the M3DW approximation predicts a three-peak structure, but with incorrect relative magnitudes between the maxima, while the MCTDW model predicts a low binary peak and no recoil structure.

In this sense, while no perfect agreement is achieved by any of the theoretical methods with the experimental data in the three emission planes for the kinematic conditions analyzed,

we observe that the SADW-EIS model improves the description of the TDCS with respect to the CDW-EIS approximation in the scattering and perpendicular planes. Nevertheless, and in concordance with what was observed for H_2O, the CDW-EIS model is the approximation that best describes this type of processes in the full-perpendicular plane.

IV. CONCLUSIONS

In this work, we have implemented two single-center approximations to the final state of the process of single ionization of molecules by electron impact: the well-known CDW, which approximates the molecular ion as a single center of charge $Z = 1$, and the SADW model, which spherically averages the anisotropic potential associated to the residual ion.

For the single ionization of H_2O at an impact energy of 65 eV, we observed that these two models are able to correctly reproduce the binary peak experimental structure, but do not yield a good prediction of the recoil peak, mainly when the magnitude of the momentum transfer increases. Besides, the SADW-EIS model overestimates the relative magnitude between the recoil and binary peak, considering emission into the full-perpendicular plane. This behavior can be attributed to an overestimation of the continuum particles interaction with the residual ion. In comparison with the M3DW approximation, we support the conclusions presented in Ref. [40], where it was suggested that the inclusion of the asymptotic Coulomb distortion in the initial channel leads to an improvement of the description of the binary region.

Considering the single ionization of THF at an impact energy of 250 eV, we observed that the SADW-EIS model slightly improves the description of the experimental data, with respect to the CDW-EIS approximation, only for electron emission into the scattering and perpendicular planes. Moreover, this seems to be the theoretical method, which achieves the best overall agreement with the experimental data for the kinematic conditions hereby analyzed.

Strikingly, and for both H_2O and THF targets, the CDW-EIS model provides the best description of the experimental structures in the full-perpendicular plane. Present results suggest that, for the geometries explored, an asymptotic physical picture of the molecular ion consisting in a single center of charge $Z = 1$, leads to a better description of the reported data compared to existing approximations that improve the description of the anisotropic potential in the vicinity of the molecular nuclei.

To summarize, present results suggest that no perfect agreement is achieved by any of the theoretical methods so far used to describe the reported data. Efforts are actually being directed in our group in order to include a multicenter description of the final state interaction in the CDW-EIS model for nonoriented complex molecular targets. Despite the fact that the calculation of TDCS is much more time consuming, as already stated, this study will hopefully let us determine the limitations of the single-center treatments shown in this work.

ACKNOWLEDGMENTS

Work at IFISUR supported by Grant No. PGI 24/F084, Secretaría General de Ciencia y Tecnología, Universidad Nacional del Sur, Argentina. We thank Dr. Xueguang Ren for providing us with the experimental data in tabular form.

[1] B. Boudaïffa, P. Cloutier, D. Hunting, M. A. Huels, and L. Sanche, Resonant formation of DNA strand breaks by low-energy (3 to 20 eV) electrons, Science **287**, 1658 (2000).

[2] M. A. Huels, B. Boudaiffa, P. Cloutier, D. Hunting, and L. Sanche, Single, double, and multiple double strand breaks induced in DNA by 3-100 eV electrons, J. Am. Chem. Soc. **125**, 4467 (2003).

[3] A. V. Solov'yov, *Nanoscale Insights into Ion-Beam Cancer Therapy* (Springer International Publishing, Berlin, 2017).

[4] E. Alizadeh, A. G. Sanz, G. Garcia, and L. Sanche, Radiation damage to DNA: The indirect effect of low-energy electrons, J. Phys. Chem. Lett. **4**, 820 (2013).

[5] K. Jung, E. Schubert, D. A. L. Paul, and H. Ehrhardt, Angular correlation of outgoing electrons following ionization of H_2 and N_2 by electron impact, J. Phys. B: Atom., Molec. Phys. **8**, 1330 (1975).

[6] M. Cherid, A. Lahmam-Bennani, A. Duguet, R. W. Zurales, R. R. Lucchese, M. C. Dal Cappello, and C. Dal Cappello, Triple differential cross sections for molecular hydrogen, both under Bethe ridge conditions and in the dipolar regime. Experiments and theory, J. Phys. B: At. Mol. Opt. Phys. **22**, 3483 (1989).

[7] L. Avaldi, R. Camilloni, E. Fainelli, and G. Stefani, Ionization of the $N_2 3\sigma_g$ orbital by electron impact studied by asymmetric (e,2e) experiments, J. Phys. B: At. Mol. Opt. Phys. **25**, 3551 (1992).

[8] J. P. Doering and J. Yang, Asymmetric (e,2e) study of the 100-eV ionization of the $3\sigma_g$ and $1\pi_u$ molecular orbitals of N_2, Phys. Rev. A **54**, 3977 (1996).

[9] S. Rioual, G. N. Vien, and A. Pochat, Ionization in coplanar symmetric (e,2e) experiments of N_2 and CO at intermediate energies, Phys. Rev. A **54**, 4968 (1996).

[10] S. J. Cavanagh and B. Lohmann, Coplanar asymmetric (e, 2e) measurements of ionization of N_2O, J. Phys. B: At. Mol. Opt. Phys. **32**, L261 (1999).

[11] J. Yang and J. P. Doering, Asymmetric (e,2e) study of the 100-eV ionization of the $1\pi_g$, $1\pi_u$ and $3\sigma_g$ molecular orbitals of O_2, Phys. Rev. A **63**, 032717 (2001).

[12] D. S. Milne-Brownlie, S. J. Cavanagh, B. Lohmann, C. Champion, P. A. Hervieux, and J. Hanssen, Dynamics in electron-impact ionization of H_2O, Phys. Rev. A **69**, 032701 (2004).

[13] C. Kaiser, D. Spieker, J. Gao, M. Hussey, A. Murray, and D. H. Madison, Coplanar symmetric and asymmetric electron impact ionization studies from the $1b_1$ state of H_2O at low to

intermediate impact energies, J. Phys. B: At. Mol. Opt. Phys. **40**, 2563 (2007).
[14] K. L. Nixon, A. J. Murray, O. Al-Hagan, D. H. Madison, and C. Ning, Low-energy symmetric coplanar and symmetric non-coplanar (e,2e) studies from the $3a_1$ state of H_2O, J. Phys. B: At. Mol. Opt. Phys. **43**, 035201 (2010).
[15] X. Ren, S. Amami, K. Hossen, E. Ali, C. G. Ning, J. Colgan, D. Madison, and A. Dorn, Electron-impact ionization of H_2O at low projectile energy: Internormalized triple-differential cross sections in three-dimensional kinematics, Phys. Rev. A **95**, 022701 (2017).
[16] J. Zhou, E. Ali, M. Gong, S. Jia, Y. Li, Y. Wang, Z. Zhang, X. Xue, D. V. Fursa, I. Bray, X. Chen, D. Madison, A. Dorn, and X. Ren, Absolute triple differential cross sections for low-energy electron impact ionization of biochemically relevant systems: Water, tetrahydrofuran, and hydrated tetrahydrofuran, Phys. Rev. A **104**, 012817 (2021).
[17] J. Ullrich, R. Moshammer, A. Dorn, R. Dörner, L. P. H. Schmidt, and H. Schmidt-Böcking, Recoil-ion and electron momentum spectroscopy: Reaction-microscopes, Rep. Prog. Phys. **66**, 1463 (2003).
[18] X. Ren, T. Pflüger, M. Weyland, W. Y. Baek, H. Rabus, J. Ullrich, and A. Dorn, An (e, 2e + ion) study of low-energy electron-impact ionization and fragmentation of tetrahydrofuran with high mass and energy resolutions, J. Chem. Phys. **141**, 134314 (2014).
[19] X. Ren, E. J. Al Maalouf, A. Dorn, and S. Denifl, Direct evidence of two interatomic relaxation mechanisms in argon dimers ionized by electron impact, Nature Commun. **7**, 11093 (2016).
[20] C. J. Colyer, S. M. Bellm, B. Lohmann, G. F. Hanne, O. Al-Hagan, D. H. Madison, and C. G. Ning, Dynamical (e, 2e) studies using tetrahydrofuran as a DNA analog, J. Chem. Phys. **133**, 124302 (2010).
[21] D. B. Jones, J. D. Builth-Williams, S. M. Bellm, L. Chiari, H. Chaluvadi, D. H. Madison, C. G. Ning, B. Lohmann, O. Ingólfsson, and M. J. Brunger, Dynamical (e,2e) investigations of tetrahydrofuran and tetrahydrofurfuryl alcohol as DNA analogues, Chem. Phys. Lett. **572**, 32 (2013).
[22] E. Wang, X. Ren, M. Gong, E. Ali, Z. Wang, C. Ma, D. Madison, X. Chen, and A. Dorn, Triple-differential cross sections for (e, 2e) electron-impact ionization dynamics of tetrahydrofuran at low projectile energy, Phys. Rev. A **102**, 062813 (2020).
[23] X. Xue, D. M. Mootheril, E. Ali, M. Gong, S. Jia, J. Zhou, E. Wang, J. X. Li, X. Chen, D. Madison, A. Dorn, and X. Ren, Triple-differential cross sections in three-dimensional kinematics for electron-impact-ionization dynamics of tetrahydrofuran at 250-eV projectile energy, Phys. Rev. A **106**, 042803 (2022).
[24] M. S. Pindzola, F. Robicheaux, S. D. Loch, and J. P. Colgan, Electron-impact ionization of H_2 using a time-dependent close-coupling method, Phys. Rev. A **73**, 052706 (2006).
[25] J. Colgan, M. S. Pindzola, F. Robicheaux, C. Kaiser, A. J. Murray, and D. H. Madison, Differential cross sections for the ionization of oriented H_2 molecules by electron impact, Phys. Rev. Lett. **101**, 233201 (2008).
[26] I. Bray, D. V. Fursa, A. S. Kadyrov, and A. T. Stelbovics, Single ionization of helium by electron impact, Phys. Rev. A **81**, 062704 (2010).
[27] X. Ren, T. Pflüger, S. Xu, J. Colgan, M. S. Pindzola, A. Senftleben, J. Ullrich, and A. Dorn, Strong molecular alignment dependence of H_2 electron impact ionization dynamics, Phys. Rev. Lett. **109**, 123202 (2012).
[28] S. D. Loch, C. J. Favreau, and M. S. Pindzola, Electron-impact ionization of the Si atom, J. Phys. B: At. Mol. Opt. Phys. **52**, 055205 (2019).
[29] M. S. Pindzola and S. D. Loch, Electron-impact ionization of the Kr atom, J. Phys. B: At. Mol. Opt. Phys. **52**, 245205 (2019).
[30] C. Granados-Castro and L. U. Ancarani, Electron impact ionization of the outer valence orbital $1t_2$ of CH_4, Eur. Phys. J. D **71**, 65 (2017).
[31] D. H. Madison and O. Al-Hagan, The distorted-wave born approach for calculating electron-impact ionization of molecules, J. At. Mol. Opt. Phys. **2010**, 367180 (2010).
[32] I. Tóth, R. I. Campeanu, and L. Nagy, Triple differential cross sections for the ionization of water by electron and positron impact, Eur. Phys. J. D **66**, 21 (2012).
[33] P. Singh, G. Purohit, C. Champion, and V. Patidar, Electron- and positron-induced ionization of water molecules: Theory versus experiment at the triply differential scale, Phys. Rev. A **89**, 032714 (2014).
[34] S. B. Zhang, X. Y. Li, J. G. Wang, Y. Z. Qu, and X. Chen, Multicenter distorted-wave method for fast-electron-impact single ionization of molecules, Phys. Rev. A **89**, 052711 (2014).
[35] M. Gong, X. Li, S. B. Zhang, S. Niu, X. Ren, E. Wang, A. Dorn, and X. Chen, Multicenter three-distorted-wave approach to three-dimensional images for electron-impact-ionization dynamics of molecules: Overall agreement with experiment, Phys. Rev. A **98**, 042710 (2018).
[36] X. Xu, M. Gong, X. Li, S. B. Zhang, and X. Chen, Theoretical study of (e, 2e) triple differential cross sections of tetrahydrofuran using multicenter distorted-wave method, J. Chem. Phys. **148**, 244104 (2018).
[37] E. Ali, H. S. Chakraborty, and D. H. Madison, Improved theoretical calculations for electron-impact ionization of DNA analogue molecules, J. Chem. Phys. **152**, 124303 (2020).
[38] C. Champion, C. Dal Cappello, S. Houamer, and A. Mansouri, Single ionization of the water molecule by electron impact: Angular distributions at low incident energy, Phys. Rev. A **73**, 012717 (2006).
[39] M. L. de Sanctis, M. F. Politis, R. Vuilleumier, C. R. Stia, and O. A. Fojón, Theoretical study of the ionization of liquid water from its several initial orbitals by fast electron impact, J. Phys. B: At. Mol. Opt. Phys. **48**, 155201 (2015).
[40] E. Acebal and S. Otranto, Continuum-distorted-wave eikonal-initial-state description of the electron-impact ionization of H_2O at low impact energies, Phys. Rev. A **98**, 012703 (2018).
[41] D. S. F. Crothers and J. S. McCaan, Ionisation of atoms by ion impact, J. Phys. B: At. Mol. Phys. **16**, 3229 (1983).
[42] P. D. Fainstein, V. H. Ponce, and R. D. Rivarola, Two-centre effects in ionization by ion impact, J. Phys. B: At. Mol. Opt. Phys. **24**, 3091 (1991).
[43] L. Gulyás, P. D. Fainstein, and A. Salin, CDW-EIS theory of ionization by ion impact with Hartree-Fock description of the target, J. Phys. B: At. Mol. Opt. Phys. **28**, 245 (1995).
[44] V. D. Rodríguez, Y. D. Wang, and C. D. Lin, Theory of longitudinal recoil-ion momentum distribution in ion-atom ionization, Phys. Rev. A **52**, R9(R) (1995).

[45] M. D. Sanchez, W. R. Cravero, and C. R. Garibotti, Internuclear potential effects on the triply differential cross section for ion-atom ionization, Phys. Rev. A **61**, 062709 (2000).
[46] J. E. Miraglia and M. S. Gravielle, Ionization of the He, Ne, Ar, Kr, and Xe isoelectronic series by proton impact, Phys. Rev. A **78**, 052705 (2008).
[47] J. E. Miraglia, Ionization of He, Ne, Ar, Kr, and Xe by proton impact: Single differential distributions in energy and angles, Phys. Rev. A **79**, 022708 (2009).
[48] J. E. Miraglia and M. S. Gravielle, Ionization of He, Ne, Ar, Kr, and Xe by impact of He^+ ions, Phys. Rev. A **81**, 042709 (2010).
[49] C. C. Montanari and J. E. Miraglia, Multiple ionization of argon by helium ions, J. Phys. B: At. Mol. Opt. Phys. **49**, 175203 (2016).
[50] N. J. Esponda, M. A. Quinto, R. D. Rivarola, and J. M. Monti, Dynamic screening and two-center effects in neutral and partially dressed ion-atom collisions, Phys. Rev. A **105**, 032817 (2022).
[51] M. F. Rojas, M. A. Quinto, R. D. Rivarola, and J. M. Monti, Dynamic effective charge in the continuum of the CDW-EIS model for ionization in ion-atom collisions: Angular and energy dependence, J. Phys. B: At. Mol. Opt. Phys. **56**, 125201 (2023).
[52] C. Champion, M. A. Quinto, J. M. Monti, M. E. Galassi, P. F. Weck, O. A. Fojón, J. Hanssen, and R. D. Rivarola, Water versus DNA: New insights into proton track-structure modelling in radiobiology and radiotherapy, Phys. Med. Biol. **60**, 7805 (2015).
[53] S. Bhattacharjee, S. Biswas, J. M. Monti, R. D. Rivarola, and L. C. Tribedi, Double-differential cross section for ionization of H_2O molecules by 4-MeV/u C^{6+} and Si^{13+} ions, Phys. Rev. A **96**, 052707 (2017).
[54] A. Bhogale, S. Bhattacharjee, M. R. Chowdhury, C. Bagdia, M. F. Rojas, J. M. Monti, A. Jorge, M. Horbatsch, T. Kirchner, R. D. Rivarola, and L. C. Tribedi, Electron emission from water vapor under the impact of 250-keV protons, Phys. Rev. A **105**, 062822 (2022).
[55] S. Jones and D. H. Madison, Evidence of initial-state two-center effects for (e, 2e) reactions, Phys. Rev. Lett. **81**, 2886 (1998).
[56] S. Jones and D. H. Madison, Ionization of hydrogen atoms by fast electrons, Phys. Rev. A **62**, 042701 (2000).
[57] S. Otranto, Initial-state correlation in the electron-impact ionization of argon, Phys. Rev. A **79**, 012705 (2009).
[58] S. Otranto and R. E. Olson, Light-particle single ionization of argon: Influence of the projectile charge sign, Phys. Rev. A **80**, 012714 (2009).
[59] O. G. de Lucio, S. Otranto, R. E. Olson, and R. D. DuBois, Triply differential single ionization of argon: Charge effects for positron and electron impact, Phys. Rev. Lett. **104**, 163201 (2010).
[60] E. Acebal and S. Otranto, Multicenter continuum-distorted-wave eikonal-initial-state description of the electron-impact ionization of aligned H_2 molecules, Phys. Rev. A **102**, 042808 (2020).
[61] R. Moccia, One-Center Basis Set SCF MO's. III. H_2O, H_2S, and HCl, J. Chem. Phys. **40**, 2186 (1964).
[62] G. M. J. Barca, C. Bertoni, L. Carrington, D. Datta, N. De Silva, J. E. Deustua, D. G. Fedorov, J. R. Gour, A. O. Gunina, E. Guidez, T. Harville, S. Irle, J. Ivanic, K. Kowalski, S. S. Leang, H. Li, W. Li, J. J. Lutz, I. Magoulas, J. Mato *et al.*, Recent developments in the general atomic and molecular electronic structure system, J. Chem. Phys. **152**, 154102 (2020).
[63] L. Fernández-Menchero and S. Otranto, Single ionization of CH_4 by bare ions: Fully differential cross sections, Phys. Rev. A **82**, 022712 (2010).
[64] L. Fernández-Menchero and S. Otranto, Fully and double differential cross sections for the single ionization of H_2O by bare ion impact, J. Phys. B: At. Mol. Opt. Phys. **47**, 035205 (2014).
[65] R. El Mir, E. M. Staicu Casasgrande, A. Naja, C. Dal Cappello, S. Houamer, and F. El Omar, Triple differential cross sections for the ionization of the valence states of NH_3 by electron impact, J. Phys. B: At. Mol. Opt. Phys. **48**, 175202 (2015).
[66] T. Khatir, S. Houamer, and C. Dal Cappello, Theoretical study of the collision dynamics in (e,2e) reactions, J. Phys. B: At. Mol. Opt. Phys. **52**, 245201 (2019).
[67] R. El Mir, K. Kaja, A. Naja, E. M. Staicu Casasgrande, S. Houamer, and C. Dal Cappello, New investigation of the electron-impact ionization of the intermediate valence state of ammonia, J. Phys. B: At. Mol. Opt. Phys. **54**, 015201 (2020).
[68] M. Attia, S. Houamer, T. Khatir, K. Bechane, and C. Dal Cappello, Electron impact ionization of atoms and molecules: An improved BBK model, J. Phys. B: At. Mol. Opt. Phys. **56**, 075201 (2023).
[69] F. Salvat, J. M. Fernández-Varea, and W. Williamson, Jr., Accurate numerical solution of the radial Schrödinger and Dirac wave equations, Comput. Phys. Commun. **90**, 151 (1995).
[70] T. Hahn, CUBA–a library for multidimensional numerical integration, Comput. Phys. Commun. **168**, 78 (2005).
[71] A. W. Malcherek and J. S. Briggs, The n-electron Coulomb continuum, J. Phys. B: At. Mol. Opt. Phys. **30**, 4419 (1997).
[72] A. Messiah, *Quantum Mechanics* (North Holland, Amsterdam, 1961), Vol. 3.
[73] L. D. Landau and E. M. Lifshitz, *Quantum Mechanics Non-Relativistic Theory* (Pergamon Press, Oxford, 1977).
[74] K. Kaufmann and W. Baumeister, Single-centre expansion of Gaussian basis functions and the angular decomposition of their overlap integrals, J. Phys. B: At. Mol. Opt. Phys. **22**, 1 (1989).
[75] L. Mouawad, P. A. Hervieux, C. Dal Cappello, J. Pansanel, A. Osman, M. Khalil, and Z. El Bitar, Triple differential cross sections for the ionization of formic acid by electron impact, J. Phys. B: At. Mol. Opt. Phys. **50**, 215204 (2017).
[76] L. Mouawad, P. A. Hervieux, C. Dal Cappello, J. Pansanel, V. Robert, and Z. El Bitar, Triple differential cross sections for the ionization of tetrahydrofuran by electron impact, J. Phys. B: At. Mol. Opt. Phys. **51**, 175201 (2018).
[77] S. J. Ward and J. H. Macek, Wave functions for continuum states of charged fragments, Phys. Rev. A **49**, 1049 (1994).